Received: 30 August 2021 | Revised: 10 November 2021 | Accepted: 31 December 2021

DOI: 10.1111/gbi.12485

ORIGINAL ARTICLE

gebiology WILEY

Growth of microaerophilic Fe(II)-oxidizing bacteria using Fe(II) produced by Fe(III) photoreduction

Ulf Lueder[1] | Markus Maisch[1] | Bo Barker Jørgensen[2] | Gregory Druschel[3] | Caroline Schmidt[1] | Andreas Kappler[1,2,4]

[1]Geomicrobiology Group, Center for Applied Geoscience (ZAG), University of Tuebingen, Tuebingen, Germany

[2]Section for Microbiology, Department of Biology, Aarhus University, Aarhus, Denmark

[3]Department of Earth Sciences, Indiana University-Purdue University, Indianapolis, Indiana, USA

[4]Cluster of Excellence: EXC 2124: Controlling Microbes to Fight Infection, Tübingen, Germany

Correspondence
Ulf Lueder, Geomicrobiology, Center for Applied Geoscience, University of Tuebingen, Schnarrenbergstrasse 94-96, D-72076 Tuebingen, Germany.
Email: lueder.ulf@gmail.com

Present address
Caroline Schmidt, Tuebingen AI Center, University of Tuebingen, Tuebingen, Germany

Funding information
Deutsche Forschungsgemeinschaft; Ministerium für Wissenschaft, Forschung und Kunst Baden-Württemberg; Bundesministerium für Bildung und Forschung

Abstract

Iron(II) (Fe(II)) can be formed by abiotic Fe(III) photoreduction, particularly when Fe(III) is organically complexed. Light-influenced environments often overlap or even coincide with oxic or microoxic geochemical conditions, for example, in sediments. So far, it is unknown whether microaerophilic Fe(II)-oxidizing bacteria are able to use the Fe(II) produced by Fe(III) photoreduction as electron donor. Here, we present an adaption of the established agar-stabilized gradient tube approach in comparison with liquid cultures for the cultivation of microaerophilic Fe(II)-oxidizing microorganisms by using a ferrihydrite-citrate mixture undergoing Fe(III) photoreduction as Fe(II) source. We quantified oxygen and Fe(II) gradients with amperometric and voltammetric microelectrodes and evaluated microbial growth by qPCR of 16S rRNA genes. We showed that gradients of dissolved Fe(II) (maximum Fe(II) concentration of 1.25 mM) formed in the gradient tubes when incubated in blue or UV light (400–530 nm or 350–400 nm). Various microaerophilic Fe(II)-oxidizing bacteria (*Curvibacter* sp. and *Gallionella* sp.) grew by oxidizing Fe(II) that was produced in situ by Fe(III) photoreduction. Best growth for these species, based on highest gene copy numbers, was observed in incubations using UV light in both liquid culture and gradient tubes containing 8 mM ferrihydrite-citrate mixtures (1:1), due to continuous light-induced Fe(II) formation. Microaerophilic Fe(II)-oxidizing bacteria contributed up to 40% to the overall Fe(II) oxidation within 24 h of incubation in UV light. Our results highlight the potential importance of Fe(III) photoreduction as a source of Fe(II) for Fe(II)-oxidizing bacteria by providing Fe(II) in illuminated environments, even under microoxic conditions.

KEYWORDS
chemical and microbial Fe(II) oxidation, cryptic cycling, cultivation, iron(II)-oxidizing bacteria, iron(III) photoreduction, microoxic

1 | INTRODUCTION

Iron (Fe) is an abundant element in aquatic and terrestrial environmental systems. Various biogeochemical interactions lead to cycling of Fe between its two main redox states +2 and +3 impacting its mobility, speciation, and bioavailability (Kappler et al., 2021). For instance, at circumneutral pH and air saturation, ferrous iron (Fe(II)) gets rapidly chemically oxidized by oxygen (O_2) and usually

precipitates as poorly soluble Fe(III) (oxyhydr)oxides (Davison & Seed, 1983; Huang et al., 2021; Millero et al., 1987; Tamura et al., 1976). The rate of Fe(II) oxidation depends, among other factors, on pH, concentration of dissolved O_2 and is catalyzed by the autocatalytic effect of Fe(III) mineral surfaces (Millero et al., 1987; Tamura et al., 1976). During the oxidation of Fe(II) by O_2, the reactive oxygen species (ROS) superoxide ($O_2^{\cdot-}$), hydrogen peroxide (H_2O_2), and hydroxyl radical ($^{\cdot}OH$) form at the stepwise reduction in O_2, which can themselves oxidize Fe(II) (Eqs. 1–4) (King et al., 1995):

$$Fe(II) + O_2 \rightarrow Fe(III) + O_2^{\cdot-} \quad (1)$$

$$Fe(II) + O_2^{\cdot-} + 2\,H^+ \rightarrow Fe(III) + H_2O_2 \quad (2)$$

$$Fe(II) + H_2O_2 \rightarrow Fe(III) + {}^{\cdot}OH + OH^- \quad (3)$$

$$Fe(II) + {}^{\cdot}OH \rightarrow Fe(III) + OH^- \quad (4)$$

Fe(II) can also be microbially oxidized, for instance at neutral pH by microaerophilic bacteria, which use Fe(II) as an electron donor and O_2 as electron acceptor for chemolithotrophic growth (Emerson et al., 2010; Emerson & Moyer, 1997). Due to competition with rapid chemical Fe(II) oxidation by O_2, these bacteria often live at oxic–anoxic interfaces with opposing gradients of Fe(II) and O_2, such as in sediments (Laufer et al., 2016), in the rhizosphere of wetland plants (Weiss et al., 2003), or at hydrothermal vents (Emerson & Moyer, 2002). There they can compete with the slow chemical reaction and contribute up to 50%–89% to the total Fe(II) oxidation (Chan et al., 2016; Neubauer et al., 2002; St Clair et al., 2019). The dynamic competition makes cultivation of microaerophilic, neutrophilic Fe(II)-oxidizing bacteria in the lab challenging; however, there are several approaches. The classical method is cultivation in agar-stabilized gradient tubes with opposing gradients of Fe(II) and O_2 (Emerson & Floyd, 2005), where microaerophilic Fe(II)-oxidizers might find their optimum growth conditions. Cultivation is also possible under microoxic conditions in Petri dishes containing zero-valent iron powder and an artificial seawater medium ("ZVI plates") (McBeth et al., 2011) or in liquid culture glass vials with $FeCl_2$ as Fe(II) source and micromolar concentrations of O_2 (Maisch et al., 2019).

In many environments, (micro)oxic and photic zones overlap. Light is therefore present at many oxic–anoxic interfaces, such as in sediments, where it can penetrate several millimeters (Kühl et al., 1994; Lueder et al., 2020). Light can drive light-induced iron cycling by serving as energy source for phototrophic Fe(II)-oxidizing bacteria (Bryce et al., 2018; Widdel et al., 1993) or by inducing Fe(III) photoreduction. During the latter process, Fe(II) is formed from reduction in organically complexed Fe(III), either by a direct ligand-to-metal charge transfer (LMCT) or by photochemically formed radicals such as superoxide (Barbeau, 2006; King et al., 1993; Rose & Waite, 2005; Sulzberger et al., 1989). Fe(III) photoreduction is an important Fe(II) source in water bodies and sediments, even at oxic conditions (Emmenegger et al., 2001; Kuma et al., 1995; Lueder, Jørgensen, et al., 2020; Miller & Kester, 1994) and phototrophic Fe(II)-oxidizing bacteria are able to oxidize Fe(II) produced by Fe(III) photoreduction (Peng et al., 2019). However, it is unknown whether microaerophilic, neutrophilic Fe(II)-oxidizing bacteria can use Fe(II) produced by photoreduction as electron donor for chemolithotrophic growth. This would enlarge their habitat to eventually oxic systems, in which, due to fast chemical Fe(II) oxidation by O_2, Fe(II) usually is not available. Fe(III) photoreduction, however, could counterbalance chemical Fe(II) oxidation in light-influenced habitats and provide Fe(II) that might be metabolized by microaerophilic Fe(II)-oxidizing bacteria enabling their growth. This could eventually even lead to a cryptic cycle if Fe redox turnover would be very quick. Therefore, the goals of this study were (i) to adapt a cultivation method for microaerophilic Fe(II)-oxidizing bacteria that exclusively utilize Fe(II) produced by Fe(III) photoreduction, (ii) to demonstrate and quantify the extent of growth of microaerophilic Fe(II)-oxidizing bacteria from Fe(II) formed by light-induced reactions under different illumination conditions, and (iii) to identify the best growth conditions for microaerophilic Fe(II)-oxidizers in gradient tubes and liquid culture glass vials based on Fe(II) produced by Fe(III) photoreduction.

2 | MATERIAL & METHODS

2.1 | Cultivation of bacteria and experimental set-up

Microaerophilic Fe(II)-oxidizing bacteria were cultivated either in agar-stabilized gradient tubes or in liquid culture glass vials. Gradient tubes were prepared based on Emerson and Floyd (2005). In 8 ml screw-cap vials, 0.75 ml of different bottom layers (stabilized with 1% (wt/vol) high-melt agarose) was overlaid by 3.75 ml top layer (stabilized with 0.15% (wt/vol) low-melt agarose). The top layer medium consisted of modified Wolfe's mineral medium (MWMM) (Emerson & Floyd, 2005) containing 0.1 g NH_4Cl, 0.2 g $MgSO_4 \times 7\,H_2O$, 0.1 g $CaCl_2 \times 2\,H_2O$ and 0.05 g K_2HPO_4 with 1 ml L^{-1} of 7-vitamin, SL10 trace metal, and selenite-tungstate solution (Pfennig, 1978; Tschech & Pfennig, 1984), adjusted to pH 6.5. The bottom layer consisted of MWMM mixed with either ferrous sulfide (FeS), 10 mM ferrihydrite, 10 mM Na-citrate, or different equimolar mixtures (1, 2, 4, 6, 8, or 10 mM each) of ferrihydrite and Na-citrate. FeS was synthesized by reaction of equimolar amounts of sulfide ($Na_2S \times 9\,H_2O$) with Fe(II) ($FeSO_4 \times 7\,H_2O$) (Lueder et al., 2018). Ferrihydrite was synthesized by adjusting the pH of a 0.2 M $Fe(NO_3)_3$ solution with 1 M KOH to 7.3 while stirring, and after 2 h without stirring, 1 M KOH was added until reaching pH 7.5. The resulting Fe(III) mineral precipitate slurry was washed four times with deionized water (MilliQ water, Milli-Q Integral System, Merck Millipore). The gradient tubes were prepared anoxically and then either pre-incubated for 1 day and illuminated with UV light (Plus lamp TVX20-ECO UVA 20W) to enable Fe(II) formation by Fe(III) photoreduction (electron donor for microaerophilic Fe(II)-oxidizers) or kept in the dark for the same duration (no Fe(II) formation). During that time, formed Fe(II) can diffuse from the bottom layer upwards. The tubes were then (after 1 day) opened (approx. 1 min) and inoculated under sterile conditions with 10 μl of a ten-fold diluted bacterial suspension sample taken from another gradient

tube with growing microaerophilic Fe(II)- oxidizers. The inoculum was inserted with a pipette that was slowly moved upward, starting to inject the inoculum just above the bottom layer. Negative controls (both pre-incubation conditions, anoxically incubated in UV light or dark) were just opened for 1 min but not inoculated with bacteria.

Liquid culture glass vials were prepared in a slightly modified way as described in Maisch et al. (2019). Briefly, 2 ml anoxic MWMM with 800 μM ferrihydrite and 800 μM Na-citrate was added to anoxic 20 ml glass vials and pre-incubated for 5 days in UV light to enable Fe(II) formation by Fe(III) photoreduction without abiotic Fe(II) oxidation by O_2. The glass vials were then inoculated with 200 μl of a ten-fold diluted microaerophilic enrichment culture grown on ZVI plates (McBeth et al., 2011), and 500 μl ambient air (at 20°C) were added leading to dissolved O_2 concentrations of 10 μM in the medium (quantified by a fiber-optic O_2 meter, see below). Negative controls were not inoculated with bacteria.

For the experiments, a microaerophilic Fe(II)-oxidizer enrichment culture from a mine (Segen Gottes Mine, Haslach im Kinzigtal, Germany) dominated by *Curvibacter* sp. (99.57% 16S rRNA gene identity to *Curvibacter delicatus*, 99.14% identity to *Leptothrix* sp.) was selected due to its robust and reproducible growth with Fe(II). *Curvibacter* spp. have only recently be identified as a novel Fe(II)-oxidizing bacterial lineage (Gülay et al., 2018). Additionally, another microaerophilic Fe(II)-oxidizing enrichment culture from Lake Constance sediment dominated by *Gallionella* sp. (Lueder et al., 2018) was selected for visual growth approval in gradient tubes.

After inoculation with Fe(II)-oxidizing bacteria and addition of O_2, gradient tubes or liquid culture glass vials were incubated without shaking at room temperature for 6 days or 96 h, respectively, in either UV light (350–400 nm plus some longer wavelength peaks, photon flux approx. 40 μmol photons m^{-2} s^{-1}), blue light (Akaiyal PAR38 15W 6000K & Lee filter 119, 400–530 nm, photon flux approx. 40 μmol photons m^{-2} s^{-1}) (Lueder et al., 2022), or in the dark. Fe(II), O_2, and H_2O_2 concentrations as well as cell growth were determined at different time points for the different incubation conditions.

2.2 | Fe(II), O_2, and H_2O_2 quantification

In gradient tubes, Fe(II) and O_2 concentrations were quantified with microsensors. Just before inoculation with bacteria, Fe(II) was quantified in gradient tubes that have anoxically been incubated in UV light or dark for 1 day, before they were then either placed in UV light, blue light, or dark. After 2 and 6 days of incubation in UV light, blue light, or dark, Fe(II) and O_2 were quantified in both inoculated gradient tubes and negative control tubes. Different gradient tubes were used at each measuring time point. For O_2 concentration gradient profiles, amperometric Clark-type O_2 microelectrodes (Unisense, Aarhus, Denmark) with 100 μm tip diameter were used. After two-point calibration in anoxic and air-saturated MWMM, O_2 profiles were recorded in triplicates in depth intervals of 2 mm using a micromanipulator (Unisense). Fe(II) concentration profiles were recorded by voltammetry using a DLK-70 potentiostat (Analytical Instrument Systems, Flemington, NJ). The standard three-electrode system consisted of a glass-encased 100 μm tip gold amalgam (Au/Hg) working electrode (Brendel & Luther, 1995), a silver wire coated with AgCl as reference electrode, and a platinum wire as counter electrode. Before measurements, working and reference electrodes were freshly plated. Calibration for Fe(II) was done with Mn(II) standards in MWMM for subsequent conversion to Fe(II) using the pilot ion method (Slowey & Marvin-DiPasquale, 2012). Fe(II) and Mn(II) were detected using cyclic voltammetry at 1000 mV s^{-1} between −0.1 and −1.8 V vs. Ag/AgCl. Initial conditioning at −0.9 V for 5 s followed by −0.05 V for 2 s removed previously precipitates on the electrode surface (Brendel & Luther, 1995). Eight scans were run at each measuring point, and the three final voltammograms were used for Fe(II) or Mn(II) quantification using VOLTINT program for Matlab® (Bristow & Taillefert, 2008). Fe(II) concentration data were recorded in 4 mm depth intervals using a micromanipulator (Unisense).

Liquid culture glass vials contained glued optode foil sensors (PSt3, PreSens, Regensburg, Germany) on the inside for non-invasive O_2 quantification using a fiber-optic oxygen meter (FiBox4, PreSens, Regensburg, Germany) that were used as described in Maisch et al. (2019). After addition of 500 μl ambient air just after inoculation with microaerophilic Fe(II)-oxidizers or in negative controls (no bacteria) to reach 10 μM dissolved O_2 in the medium, O_2 was only checked again at the end of the experiment to ensure similar O_2 concentrations over the course of the experiment. Sampling for Fe and H_2O_2 was done in triplicate set-ups just at the start of the experiment as well as after 6, 24, 48, 72, and 96 h of incubation in UV light, blue light, or dark. Fe(II), total Fe (Fe_{tot}), and H_2O_2 were spectrophotometrically quantified using the ferrozine assay (Stookey, 1970) or leuco crystal violet assay (Cohn et al., 2005; Mottola et al., 1970), respectively. Briefly, samples for Fe were fixed in 1 M HCl to prevent Fe(II) oxidation prior to analysis. Samples for H_2O_2 were added to EDTA (10 mM final concentration) to chelate Fe(II) and avoid reaction with H_2O_2. 100 mM KH_2PO_4, 41 μM leuco crystal violet, and 1 μg (0.18 units) horseradish peroxidase were added, and absorbance at 592 nm was measured in triplicates after 1 day.

2.3 | Cell visualization and quantification of growth

The growth of Fe(II)-oxidizing bacteria in gradient tubes was confirmed by the presence of visually distinct brownish Fe(III) mineral precipitation in the top layer (3.75 ml MWMM stabilized with 0.15% (wt/vol) low-melt agarose) of gradient tubes as a clear differentiation from the negative control tubes, in which the distinct brownish Fe(III) mineral precipitations do not form (Emerson & Floyd, 2005; Lueder et al., 2018). Additionally, subsamples from these precipitates were stained with LIVE/DEAD® *Bac*Light™ fluorescent dye and the presence of living cells was confirmed by fluorescence microscopy. For detection of close cell–mineral interactions, samples for scanning electron microscopy (SEM) were taken from Fe(III) mineral precipitates in inoculated gradient tubes with a ferrihydrite-citrate mixture in the bottom layer (8 mM each) after 6 days incubation in UV light.

A volume of 1 ml sample was mixed with 50 µl anoxic glutaraldehyde (4°C), 100 µl anoxic paraformaldehyde (20%), and 200 µl anoxic PIPES buffer (100 mM) solution for chemical fixation. The mixture was then stored at 4°C for 24 h. After fixation, an aliquot was transferred onto a glass slide (diameter 0.5 cm) which was previously coated with poly-L-lysin (5%). The sample was allowed to rest for 10–15 min for cells and mineral particles to settle onto the glass slide. Subsequently, water was removed from the sample by dehydration in ethanol solutions with increasing concentrations from 15, 30, 50, 70, 80, 90, 96 to 100 vol-% for 10 min each. After the 100% ethanol wash, the glass slide was transferred into hexamethyldisilazane (HMDS) to preserve cell integrity during air drying of the sample. The glass slide was then dried at room temperature in the fume hood and transferred onto an aluminum stub with adhesive carbon tape. Before transfer into the scanning electron microscope, all samples were sputter-coated with platinum (layer thickness 8 nm). Image acquisition was performed on a FIB-SEM (Crossbeam 550L, Zeiss, Germany) in high-resolution imaging mode with electron high tension (EHT) of 5 kV, working distance (WD) of 5 mm, probe current (IProbe) of 50 pA, dwell time of 50 ns, and a secondary electrons secondary ions (SESI) detector.

Cell growth was quantified in gradient tubes and liquid culture glass vials with quantitative polymerase chain reaction (qPCR) of 16S rRNA genes. The whole top layer from gradient tubes with a ferrihydrite-citrate mixture bottom layer (8 mM) was homogenized by transferring and mixing it with a pipette, and 1 ml of homogenized top layer was sampled in triplicate set-ups shortly after inoculation as well as after 6 days incubation in UV light, blue light, or dark and diluted with 1 ml MilliQ. 1.5 ml of liquid culture in glass vials was sampled just after inoculation as well as after 48 h and 96 h of incubation in UV light, blue light, or dark. Samples were frozen until further processing. DNA was extracted using the DNeasy UltraClean Microbial Kit (Qiagen, Hilden, Germany) following the instructions of the manufacturer. 16S rRNA quantification was done using the CFX96 Real-Time PCR detection system and CFX maestro software (Bio-Rad laboratories, Hercules, CA, USA) as well as the 341 F and 797 R primer pair (Nadkarni et al., 2002). Plasmids containing the respective genes were used as standards for calibration and quantified fluorometrically with Qubit 2.0 (Invitrogen, Carlsbad, CA, USA). qPCR was done in triplicates in 96-well plates with 10 µl containing SsoAdvanced™ Universal SYBR® Green Supermix (Bio-Rad laboratories), 341 F (75 nM), 797 R (225 nM) primers, and 1 µl DNA template.

2.4 | Kinetic calculations

The rate of Fe(II) oxidation, $\frac{dc}{dt}$, in liquid culture glass vials between the different sampling intervals was calculated by dividing the change of Fe(II) concentration over the sampling interval by the duration of the interval (from time 0 h to time *x* h). The microbial contribution to the overall Fe(II) oxidation in liquid culture glass vials for 24 and 48 h incubation in UV light after inoculation with *Curvibacter* sp. was determined by comparing Fe(II) removal in inoculated (biotic) with uninoculated vials (abiotic) by the following equation (Eq. 5):

$$\text{Microbial contribution} = \frac{\left(\left[\text{Fe(II)}\right]_{0\text{ h, biotic}} - \left[\text{Fe(II)}\right]_{x\text{ h, biotic}}\right) - \left(\left[\text{Fe(II)}\right]_{0\text{ h, abiotic}} - \left[\text{Fe(II)}\right]_{x\text{ h, abiotic}}\right)}{\left(\left[\text{Fe(II)}\right]_{0\text{ h, biotic}} - \left[\text{Fe(II)}\right]_{x\text{ h, biotic}}\right)} \cdot 100\ \% \quad (5)$$

3 | RESULTS

3.1 | Fe(III) mineral precipitation and growth of Fe(II)-oxidizing bacteria in gradient tubes

We identified microbial growth in the gradient tubes by observing visually the morphology of Fe(III) mineral precipitates and by microscopy. While abiotic Fe(II) oxidation by O_2 usually produce a diffuse, brownish discoloration in the top layer of gradient tubes, distinct brownish Fe(III) mineral precipitates form as a result from the activity of microaerophilic Fe(II)-oxidizing bacteria (Emerson & Floyd, 2005). Two days after microbial inoculation in gradient tubes with equimolar ferrihydrite-citrate mixtures (4, 6, 8, 10 mM each, incubation in UV light) or with FeS bottom layers and with air in the headspace, we observed the formation of these distinct brownish precipitates, which clearly differed from negative, that is, uninoculated control tubes (Figure 1A–D). We used inoculated FeS bottom layer gradient tubes (Figure 1A,C) as "positive" control for growth of the *Curvibacter* sp. enrichment culture as this is a common and reliable cultivation method for microaerophilic Fe(II)-oxidizing bacteria (Emerson & Floyd, 2005; Lueder et al., 2018). No visible brown mineral precipitates formed in inoculated gradient tubes containing ferrihydrite-citrate mixtures of either 1 or 2 mM each or in gradient tubes containing either 10 mM ferrihydrite or 10 mM citrate bottom layers (Figure 1A,C). Furthermore, besides in FeS gradient tubes, which serve as biotic controls for growth, no brownish precipitates were observed in inoculated gradient tubes when incubated in dark (Figure 1B,D). Chemically formed brownish mineral precipitates (both in negative control tubes with ferrihydrite/citrate and in FeS gradient tubes) appeared more diffuse and less distinct than in inoculated tubes (Figure 1A–D).

Precipitation of brown minerals in the top layer of gradient tubes containing Fe(III) in the bottom plug (in the form of ferrihydrite-citrate mixtures) implies that Fe(III) was photoreduced to Fe(II) by UV light. The Fe(II) then diffused upwards and precipitated as Fe(III) mineral due to abiotic Fe(II) oxidation and by microaerophilic Fe(II)-oxidizing bacteria using O_2 diffusing down from the headspace. The position of the Fe(III) mineral precipitates, which indicate growth of microaerophilic Fe(II)-oxidizing bacteria, depended on concentrations of ferrihydrite-citrate in the bottom layers. The precipitates found in gradient tubes inoculated with a *Curvibacter* sp. enrichment culture were positioned closest to the bottom layer in gradient tubes with a 4 mM (each) ferrihydrite-citrate mixture bottom layer, while at

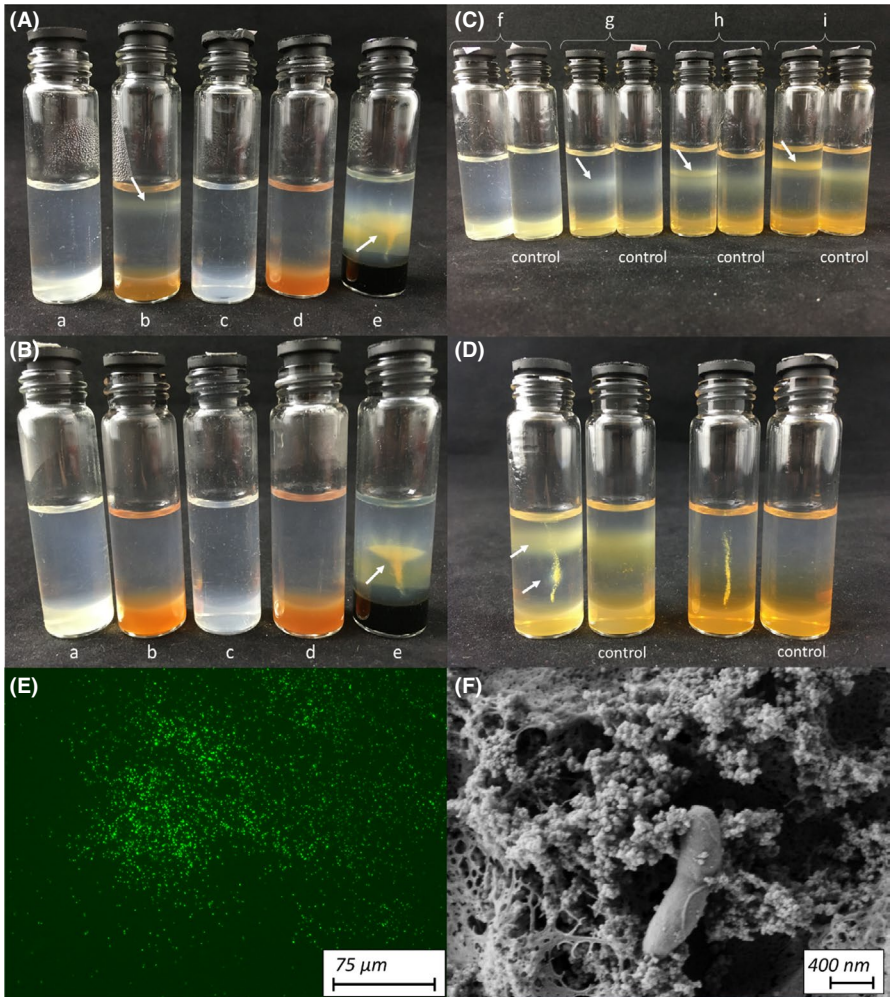

FIGURE 1 Visual observations of cell growth in gradient tubes. (A, B) Gradient tubes inoculated with a *Curvibacter* sp. enrichment culture containing different bottom plugs. a: mixture of 1 mM ferrihydrite and 1 mM citrate, b: mixture of 10 mM ferrihydrite and 10 mM citrate, c: 10 mM citrate, d: 10 mM ferrihydrite, e: FeS, either incubated for 3 days in UV light (A) or dark (B). Formation of typical growth bands produced by microaerophilic Fe(II)-oxidizers (indicated by white arrows) was observed in tubes b (UV incubation) and e (UV and dark incubation). (C) Gradient tubes inoculated with a *Curvibacter* sp. enrichment culture and uninoculated (abiotic) controls containing bottom plugs with a mixture of f: 2 mM ferrihydrite and 2 mM citrate, g: 4 mM ferrihydrite and 4 mM citrate, h: 6 mM ferrihydrite and 6 mM citrate, and i: 8 mM ferrihydrite and 8 mM citrate. The position of the growth bands (indicated by white arrows) in inoculated gradient tubes varies with Fe concentrations of the bottom plug. (D) Gradient tubes with a bottom plug containing a mixture of 8 mM ferrihydrite and 8 mM citrate either inoculated with a *Gallionella* sp. enrichment culture or uninoculated controls. The two left gradient tubes were incubated in UV light for 4 days, and the two right were kept in dark for 4 days. Formations of a cell growth band and cloudy mineral precipitates are indicated by white arrows. (E, F) Fluorescence (E) and scanning electron (F) microscopy images of samples taken from growth bands in UV-incubated gradient tubes (8 mM citrate-ferrihydrite mixture bottom plug) showing bacterial cells from a *Curvibacter* sp. enrichment culture (E, F), Fe minerals and agarose residuals (F)

10 mM precipitates formed near the top of the liquid medium, close to the air headspace (Figure 1A,C). The shape of the mineral precipitation band depended on the bottom layer. While in ferrihydrite-citrate mixture gradient tubes, a sharp horizontal band formed in UV incubation (Figure 1A,C), a funnel-like structure formed in FeS gradient tubes in UV and dark incubations (Figure 1A,B). Gradient tubes (8 mM ferrihydrite-citrate mixture bottom layers) incubated in UV light and inoculated with a non-diluted *Gallionella* sp. enrichment showed a slightly diffuse horizontal band and diffuse brownish cloudy precipitates around the inoculum that did not form in negative control tubes or in dark incubation (Figure 1D).

Fluorescence microscopy analysis of samples taken from the brownish precipitates in a gradient tube containing a *Curvibacter* sp. enrichment culture showed a high number of living cells (Figure 1E), and SEM revealed close associations between cells and Fe minerals (Figure 1F). As most distinct brownish precipitates formed in UV-incubated gradient tubes with an 8 mM (each) ferrihydrite-citrate mixture bottom layer, growth of a *Curvibacter* sp. enrichment culture in those tubes was quantified after 6 days of incubation in UV light (more energy), in blue light (less energy), and in the dark based on 16S rRNA gene copy numbers using qPCR (Figure 2). While directly after inoculation, number of gene copies was close to the

limit of detection, it increased after 6 days to approx. 6×10^7 ml^{-1} in UV-incubated gradient tubes, to 4×10^7 ml^{-1} in blue light, and to 6×10^6 ml^{-1} in dark incubated gradient tubes (Figure 2B). These numbers relate to the visual appearance of brownish precipitates: A sharp and distinct band formed in gradient tubes during UV incubation, a diffuse and vague band formed during blue light incubation, and no band was visible during incubation in the dark (Figure 2A).

3.2 | Development of Fe(II) and O_2 gradients in gradient tubes

Gradients of dissolved Fe(II) and O_2 concentrations were monitored over time by microelectrode measurements in gradient tubes containing a ferrihydrite-citrate mixture (8 mM each) bottom layer (Figure 3). Before opening the tubes (i.e., filling the headspace with ambient air) and/or inoculating them with a *Curvibacter* sp. enrichment culture, the tubes were either pre-incubated anoxically in UV light for 1 day to photochemically form Fe(II) (up to 750 μM formed close to the bottom layer and decreased to 50 μM near the top of the liquid medium, close to the air headspace (Figure 3a) or kept in the dark to avoid light-induced Fe(II) formation (Figure 3b). In those dark pre-incubated tubes, maximum Fe(II) concentrations of only 100 μM formed close to the bottom layer (Figure 3b), probably due to some light-exposure during the gradient tube preparation or during measurements. Directly after inoculation with bacteria and/or exposure to O_2 (negative controls), UV pre-incubated gradient tubes were incubated in UV light or in blue light while dark pre-incubated gradient tubes were incubated in dark.

After 2 days of incubation, O_2 penetrated from the headspace down to 12 mm in UV and blue light incubated gradient tubes (in both, inoculated and control tubes) (Figure 3c,d) and reached the bottom layer in dark incubated gradient tubes (Figure 3e). Incubated in UV light, in inoculated gradient tubes, brownish precipitates became visible in the top layer at 6–7 mm beneath the air–liquid interface and O_2 concentrations were slightly lower than in control tubes (Figure 3c). The Fe(II) concentration close to the bottom layer reached 1250 μM (UV light incubation) and 850 μM (blue light incubation), respectively, while Fe(II) was not detectable in the upper 8 mm of the top layer (Figure 3c,d). After 6 days of incubation, no Fe(II) was detected in the top layer and O_2 reached the bottom layer in all control tubes at any incubation condition (Figure 3f–h). Only in inoculated gradient tubes incubated under UV or blue light and with visual brownish precipitates (and consequently growth of Fe(II)-oxidizing bacteria) (Figure 2), Fe(II) concentrations close to the bottom layers reached up to 800 μM (UV light) or 400 μM (blue light) and had decreasing concentrations upwards (Figure 3f,g). In those gradient tubes, O_2 penetrated 6–8 mm down from the air headspace into the top layer (Figure 3f,g). During UV incubation, no O_2 was detected below and no Fe(II) was detected above the brownish band of mineral precipitations (Figure 3f).

3.3 | Growth of Fe(II)-oxidizing bacteria and geochemical conditions in liquid culture glass vials

Additionally to the use of gradient tubes, we cultivated a *Curvibacter* sp. enrichment culture in liquid culture as this set-up allows kinetic calculations and quantification of the microbial contribution to the overall Fe(II) oxidation. Illumination of anoxic liquid culture glass vials containing 800 μM ferrihydrite and 800 μM Na-citrate with UV light for 5 days led to 80% transformation of the Fe(III) to Fe(II). After addition of ambient air, resulting in a dissolved O_2 concentration of 10 μM, the Fe(II) concentration decreased due to Fe(II) oxidation. In the dark, Fe(II) was completely oxidized within 48 h in both inoculated (*Curvibacter* sp. enrichment) and uninoculated control vials (Figure 4a). Fe(II) oxidation was fastest in the first 6 h (40–50 μM h^{-1}) after addition of air and slowed down to near-zero μM h^{-1} after 24 h (Figure 4b). Within the first 48 h in the dark, H_2O_2 accumulated, peaked at 4 μM 6 h after aeration, and subsequently decreased in inoculated and negative control vials (Figure 4c). In blue light incubation, Fe(II) removal was slightly retarded compared to dark incubation (Figure 4a) but the rate of Fe(II) oxidation followed the same trend with fastest rates being in the first 6 h after air addition

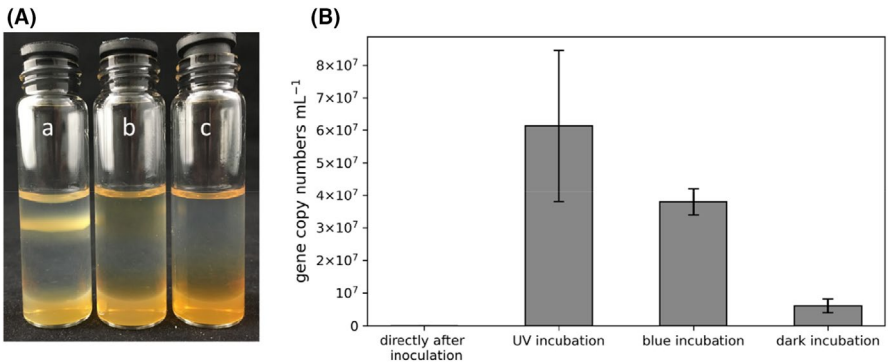

FIGURE 2 (A) Gradient tubes (bottom plug mixture 8 mM ferrihydrite and 8 mM citrate) with a *Curvibacter* sp. enrichment culture incubated for 6 days in UV light (a), blue light (b), or dark (c). (B) qPCR quantification of 16S rRNA genes from triplicate gradient tubes directly after inoculation and after 6 days incubation in UV light, blue light, or dark (as seen in (A)). Error bars represent the standard deviation of results from 3 gradient tubes

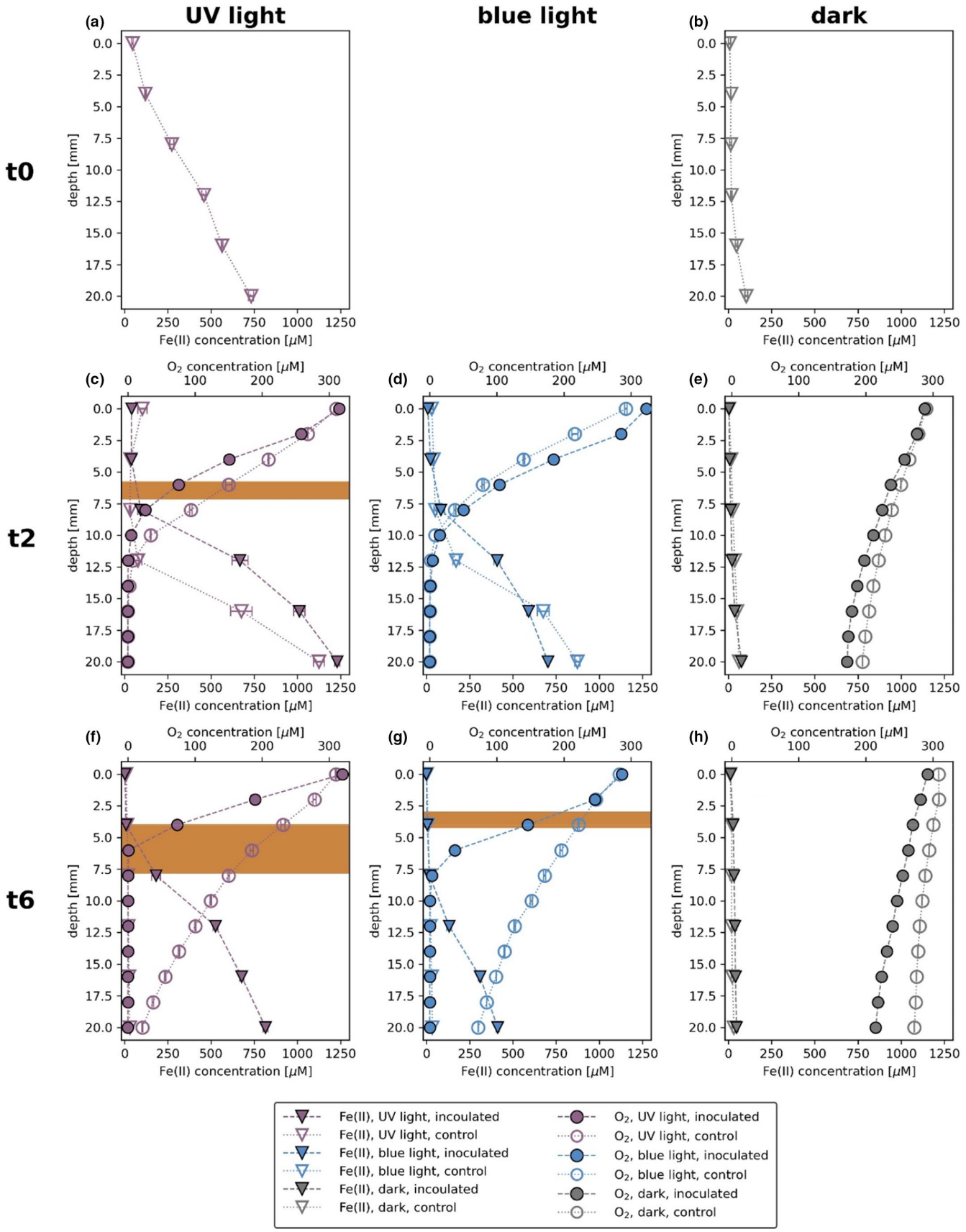

FIGURE 3 Microelectrode O_2 (circles) and Fe(II) (triangles) concentration profiles at different time points (t0: before incubation; t2: 2 days of incubation; t6: 6 days of incubation) and incubation conditions (UV light (a, c, f); blue light (d, g); dark (b, e, h)) in gradient tubes (bottom plug mixture 8 mM ferrihydrite and 8 mM citrate) inoculated with a *Curvibacter* sp. Enrichment culture (filled symbols) or uninoculated controls (open symbols). Formation of a typical growth band formed by microaerophilic Fe(II)-oxidizers is indicated by a brown box. Error bars represent the standard deviation of the triplicate measurements/voltammograms

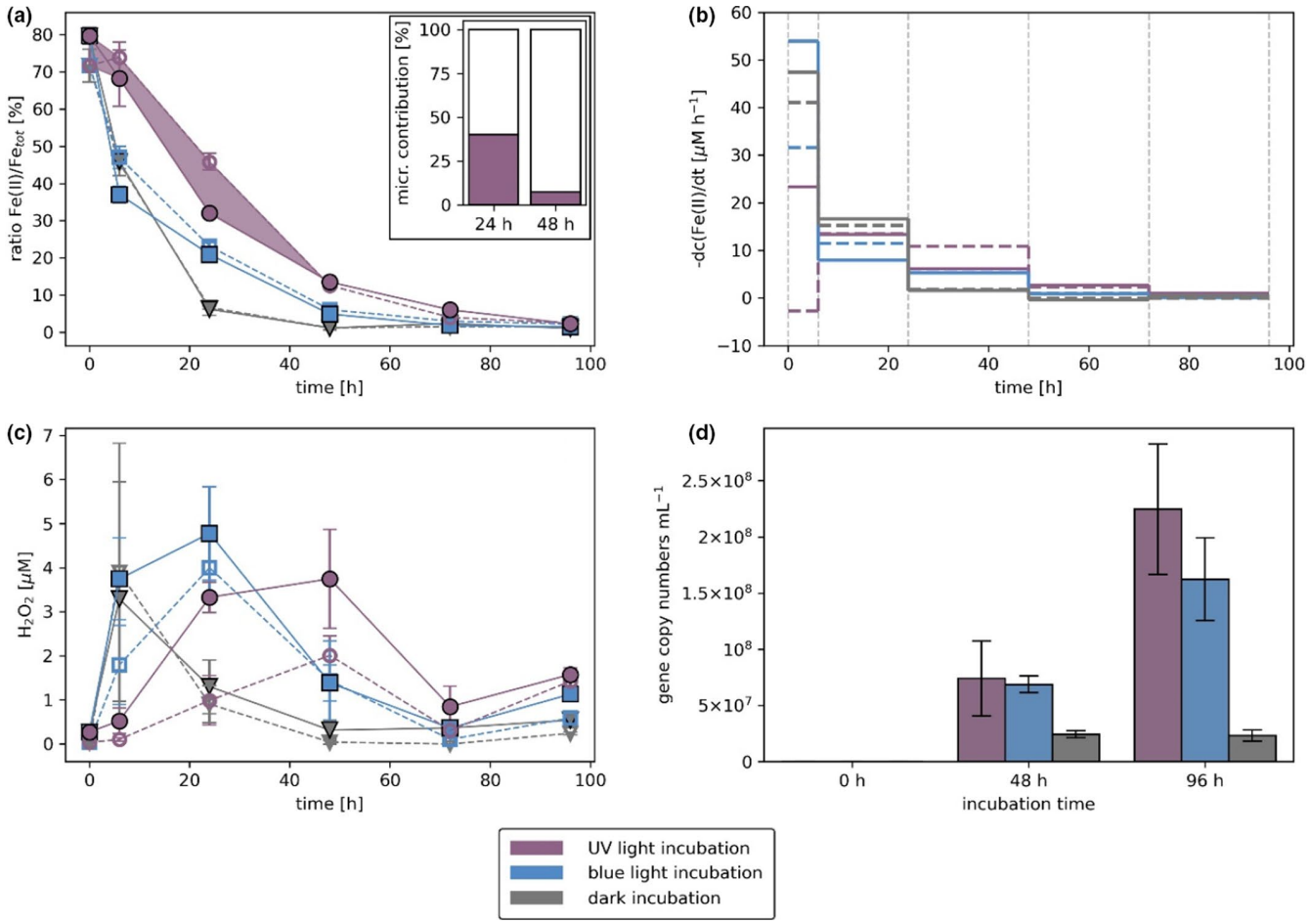

FIGURE 4 Liquid culture experiments at different incubation conditions (UV light, blue light, and dark incubation). (a, c) Fe(II)/Fe$_{tot}$ ratio (a) and H_2O_2 concentration (c) over time in glass vials inoculated with a *Curvibacter* sp. enrichment culture (filled symbols, solid lines) or uninoculated controls (open symbols, dashed lines). The microbial contribution to the overall Fe(II) oxidation is indicated by the shaded area between the purple curves showing the Fe(II)/Fe$_{tot}$ development in glass vials incubated in UV light and in the inset shown in (a). (b) calculated rate of change of Fe(II) concentration over time for different time intervals in glass vials inoculated with a *Curvibacter* sp. enrichment culture (solid lines) or uninoculated controls (dashed lines). (d) 16S rRNA gene copy numbers from triplicate glass vials at the beginning (0 h) and after 48 and 96 h incubation in UV light, blue light, or dark. Error bars represent the standard deviation of results from 3 glass vials

(30–55 μM h^{-1}) (Figure 4b). H_2O_2 accumulated up to 5 μM after 24 h incubation and persisted longer in light than in dark incubation (Figure 4c). Also, slightly more H_2O_2 accumulated in inoculated glass vials than in uninoculated controls (Figure 4c). UV light incubation led to the slowest drop in Fe(II), with Fe(II) still being detected 72 h after addition of air (Figure 4a). Within the first 48 h of incubation, Fe(II) was higher in control vials compared to inoculated vials and even slightly increased in the first 6 h (Figure 4a). UV light incubation led to slower Fe(II) decrease in the first 6 h (approx. 23 μM h^{-1}) after aeration or some Fe(II) production (approx. 3 μM h^{-1}) in negative control vials, but the rate of the Fe(II) oxidation showed afterward a similar trend as the other incubation conditions (Figure 4b). H_2O_2 accumulated up to 4 μM after 48 h of incubation with higher H_2O_2 concentrations in inoculated vials than in negative controls (Figure 4c). During UV light incubation, contribution of Fe(II)-oxidizing bacteria to the overall Fe(II) oxidation was approx. 40% 24 h after addition of air but decreased to only 8% during the following 24 h (Figure 4a inset). Cell growth (*Curvibacter* sp. enrichment) was quantified based on 16S rRNA gene copy numbers. 16S rRNA gene copy numbers increased to approx. 7×10^7 ml^{-1} after 48 h and to 2.3×10^8 ml^{-1} after 96 h incubation in UV light. In blue light, 16S rRNA gene copy numbers also increased to approx. 7×10^7 ml^{-1} after 48 h and then to 1.6×10^8 ml^{-1} another 48 h later. (Figure 4d). Gene copies in dark only slightly increased to 2.4×10^7 ml^{-1} 48 h after addition of air and stayed constant until the end of incubation (Figure 4d).

4 | DISCUSSION

4.1 | Formation of Fe(II) by Fe(III) photoreduction

For cultivation of microaerophilic Fe(II)-oxidizing bacteria in gradient tubes, different Fe(II) sources such as FeS, Fe^0, $FeCl_2$, or $FeCO_3$ can be added to the bottom layer (Emerson & Moyer, 1997; Kato

et al., 2012; Lueder et al., 2018; Macdonald et al., 2014; Swanner et al., 2011). To ensure that all available Fe(II) was produced by Fe(III) photoreduction, we selected a mixture of Fe(III) (in the form of ferrihydrite) and citrate as organic ligand. Fe(III) photoreduction of inorganic Fe(III) species is insignificant at circumneutral pH (King et al., 1993), but citrate forms photo-susceptible complexes with Fe(III) that readily undergo Fe(III) photoreduction upon exposure to blue or UV light (Dou et al., 2021; Faust & Zepp, 1993). During anoxic incubation in UV light, Fe(II) was most probably formed by LMCT reactions during which an electron is transferred from citrate to complexed Fe(III) (Kuma et al., 1995), with accompanying decarboxylation of citrate (Abrahamson et al., 1994; Bennett et al., 1982). Fe(III)–citrate complexes diffused upwards from the bottom to the top layer and got photoreduced there and/or Fe(II) diffused upwards, which was photoproduced already within the bottom layer. This resulted in an Fe(II) gradient built up in the tubes that have been placed for 1 day in UV light with maximum concentrations of approx. 750 μM close to the bottom layer (Fe_{tot} 8 mM) (Figure 2A).

By adding air to the headspace of gradient tubes, (chemical) Fe(II) oxidation took place in the top layer as O_2 diffused downwards. In gradient tubes that were incubated in UV or blue light, Fe(III) photoreduction continued to take place leading to higher concentrations of Fe(II) of up to 1250 μM close to the bottom layer 2 days after bacteria inoculation and addition of ambient air (Figure 2C,D). Fe(II) concentrations in UV light were higher than in blue light as UV has more energy and is therefore more efficient by Fe(III) photoreduction (Lueder et al., 2022; Pehkonen et al., 1993; Rijkenberg et al., 2005). Over time, O_2 reached the bottom layer of negative control tubes in UV and blue light incubation, that is, the chemical oxidation rate of Fe(II) was higher than the Fe(III) photoreduction rate of Fe(III)–citrate leading to a complete removal of Fe(II) 6 days after addition of ambient air (Figure 3f,g). This could also be due to the lack of available Fe(III)–citrate complexes in the top layer due to slower diffusion of Fe(III)–citrate or Fe(II) compared to diffusion of O_2. According to Dou et al. (2021), the diffusivity factor (normalized to water) of O_2 is larger than the diffusivity factors of Fe(II) and Fe(III)–citrate. Interestingly, O_2 did not reach the bottom of the inoculated gradient tubes in UV and blue light incubation after 6 days (as it did in the negative control tubes) but only penetrated 10–12 mm into the top layer from the air headspace (Figure 3f,g). This is probably the case because microbial Fe(II) oxidation took place in addition to chemical Fe(II) oxidation thus consuming all O_2 before it could penetrate into deeper layers. However, Fe(III) photoreduction and diffusion of Fe(III)–citrate or Fe(II) from the bottom layer are obviously sufficient in those gradient tubes to deliver Fe(II) to the oxic–anoxic interface and to maintain anoxic conditions in the lower regions of the top layer (Figure 3f,g).

The production of Fe(II) by photoreduction of Fe(III)–citrate was adapted for cultivation of microaerophilic Fe(II)-oxidizers in liquid culture in microoxic glass vials (Maisch et al., 2019). Anoxic incubation without bacteria for 5 days in UV light led to Fe(II) production via Fe(III) photoreduction corresponding to 80% of the total available Fe. As not all Fe(III) was reduced to Fe(II), reactive Fe(III) mineral surfaces (ferrihydrite) were still present in the medium. Those iron mineral surfaces can serve as catalyst for fast heterogenous Fe(II) oxidation, strongly speeding up the chemical Fe(II) oxidation; during slower, homogeneous Fe(II) oxidation, dissolved Fe(II) is oxidized by dissolved O_2 (Barnes et al., 2009; Park & Dempsey, 2005; Tamura et al., 1976). This explains the complete removal of Fe(II) in dark incubation already 48 h after addition of air (Figure 4a). Maisch et al. (2019) showed that Fe(II) was stable at 10 μM O_2 for a longer time when Fe(III) minerals such as ferrihydrite were not present at the start of their experiment. By that, no heterogeneous, but only homogeneous, Fe(II) oxidation took place in the initial phase of the incubation when all Fe was dissolved and showed the accelerating effect of mineral surfaces on kinetics of Fe(II) oxidation.

In liquid culture, illumination and the resulting Fe(III) photoreduction increased the availability of Fe(II) until 72–96 h after addition of air (Figure 4a). UV light provided more Fe(II) due to high Fe(III) photoreduction rates (Lueder et al., 2022; Pehkonen et al., 1993; Rijkenberg et al., 2005), and by that provided an advantage for the microaerophilic Fe(II)-oxidizers compared to the other incubation conditions. This can be seen from the high microbial contribution (40%) to the overall Fe(II) oxidation during the first 24 h after inoculation (Figure 4a inset). A side effect of illumination was higher and longer lasting accumulation of H_2O_2 in liquid culture vials compared to dark incubation (Figure 4c). This H_2O_2 most probably formed during chemical oxidation of Fe(II) (Eq. 2). In light incubation, Fe(II) was constantly photoproduced and, consequently, more Fe(II) oxidation took place in total, resulting in formation and accumulation of higher H_2O_2 concentrations.

In gradient tubes and liquid culture glass vials containing ferrihydrite and citrate, Fe(III) photoreduction generally did not only deliver Fe(II) but also increased its persistence and availability by constantly re-forming Fe(II). This Fe(II) then was used as electron donor by the microaerophilic Fe(II)-oxidizers resulting in bacterial growth.

4.2 | Growth of microaerophilic Fe(II)-oxidizers using photoproduced Fe(II)

Visual confirmation of growth of microaerophilic Fe(II)-oxidizing bacteria can easily be done in gradient tubes due to the formation of distinct brownish precipitates (Emerson & Floyd, 2005; Lueder et al., 2018). We did not observe these precipitates in gradient tubes without or with only low production of Fe(II), that is, containing only ferrihydrite, only citrate, or ferrihydrite-citrate concentrations below 4 mM each, or in gradient tubes incubated in the dark (Figure 1A–D). In gradient tubes containing sufficient Fe(II) (ferrihydrite-citrate mixtures with concentrations of 4–10 mM each, illuminated with UV light), distinct brownish precipitates formed (i.e., Fe(II)-oxidizers grew) (Figure 1A–D). The position of these characteristic and distinct growth bands depended on the Fe(II) or O_2 gradients. At higher ferrihydrite-citrate concentrations, steeper Fe(II) gradients with higher Fe(II) concentrations close to the bottom layer formed in light

in the top layer. The depth of O_2 penetration depended on the Fe(II) gradient in the top layer due to consumption of O_2 by chemical and microbial Fe(II) oxidation. The microaerophiles grow in these gradient tubes at a position where sufficient Fe(II) is available and where they can compete with the kinetics of chemical Fe(II) oxidation by O_2, which is considered to be below 50 μM O_2 (Druschel et al., 2008). We showed that different microaerophilic Fe(II)-oxidizing bacteria (*Curvibacter* sp. and *Gallionella* sp.) are able to grow in gradient tubes utilizing Fe(II) produced by Fe(III) photoreduction. UV illumination could have negatively affected the growth of Fe(II)-oxidizing bacteria as UV light damages DNA. Nevertheless, most cell growth was quantified at the UV-illumination conditions (Figure 2B, Figure 4d). Eventually, prevalent Fe(III) minerals likely protected the microaerophilic Fe(II)-oxidizing bacteria by shielding from the UV light (Gauger et al., 2015, 2016).

Fe(III) photoreduction induced by UV or blue light could not deliver sufficient Fe(II) to counterbalance abiotic Fe(II) oxidation over longer times. Concentrations of Fe(II) therefore decreased over time. This can be explained by a decreasing availability of citrate (which gets decarboxylated during Fe(III) photoreduction (Abrahamson et al., 1994)) that can form photo-susceptible Fe(III)–citrate complexes and by increasing Fe(II) oxidation rates due to increasing heterogenous Fe(II) oxidation (Park & Dempsey, 2005; Tamura et al., 1976). Nevertheless, Fe(III) photoreduction of Fe(III)–citrate by UV or blue light enabled Fe(II)-oxidizing bacteria to grow over several days in gradient tubes (Figure 1, Figure 2) or liquid culture glass vials (Figure 4) despite the very different growth conditions found by these two cultivation methods.

4.3 | Optimum growth conditions in gradient tubes and liquid culture glass vials

Microaerophilic Fe(II)-oxidizing bacteria have been grown in both agar-stabilized gradient tubes and liquid culture glass vials (Emerson & Floyd, 2005; Emerson & Moyer, 1997; Kato et al., 2012; Macdonald et al., 2014; Maisch et al., 2019; Swanner et al., 2011). A general advantage of gradient tubes is the development of dynamic Fe(II) and O_2 gradients (Druschel et al., 2008; Lueder et al., 2018), in which different microaerophilic Fe(II)-oxidizers might find optimum growth conditions, depending on their specific requirements. When using ferrihydrite-citrate mixtures in the bottom layer, concentrations of 8 mM each apparently provided the best conditions for growth of microaerophilic Fe(II)-oxidizers during incubation in UV light, as judged from the optical density and sharpness of the growth band (Figure 1C). UV light was clearly a more suitable illumination for growth than blue light because (a) more gene copy numbers were quantified for *Curvibacter* sp. after several days of growth (Figure 2B, Figure 4d), (b) visible brownish precipitates in the top layer of gradient tubes appeared earlier (after 2 days), and (c) Fe(II) persisted longer (Figure 4a). Illumination with UV or blue light was adjusted to the same photon flux (40 μmol photons m^{-2} s^{-1}), which might be found upper sediment layers depending on weather conditions and overlying water (Jørgensen et al., 1987; Kühl et al., 1994; Lueder, Jørgensen, et al., 2020). However, the effect of different photon fluxes for Fe(III) photoreduction efficiency was not tested in this study. Generally, a higher photon flux leads to higher light-induced Fe(II) production rate (Kuma et al., 1995; Lueder et al., 2022; Waite et al., 1995). It is therefore possible that different photon fluxes than used in this study would have led to even better growth conditions, for example, by producing more Fe(II) due to higher Fe(III) photoreduction rates, thereby leading to higher Fe(II) concentrations or longer Fe(II) persistence times. Addition of more citrate could also prolong the persistence and availability of Fe(II) for microaerophilic Fe(II)-oxidizing bacteria and consequently improve their growth conditions. During Fe(III) photoreduction, Fe(III) gets reduced and citrate gets decarboxylated to acetone dicarboxylic acid with the ultimate decarboxylation product being acetone (Abrahamson et al., 1994), which cannot complex Fe(III). As long as sufficient citrate is available, it can form fresh dissolved Fe(III)–citrate complexes and prevent precipitation of poorly soluble Fe(III) (oxyhydr)oxides. Fe(III) photoreduction can thereby proceed, forming more Fe(II). This implies that less Fe(III) mineral surfaces are available, which retards heterogenous Fe(II) oxidation.

Based on cell numbers, cultivation of microaerophilic Fe(II)-oxidizers in liquid culture glass vials appears to provide better growth conditions than gradient tubes as higher gene copy numbers were quantified and the cells grew in a shorter incubation time (96 h in liquid culture vs. 6 days in gradient tubes). Numbers of 16S rRNA gene copies were an order of magnitude higher in liquid culture vials (10^8 ml^{-1} vs. 10^7 ml^{-1}) (Figure 2B, Figure 4d). However, bacteria were inoculated differently (10 μl inoculum in gradient tubes vs. 200 μl (10%) inoculum in liquid culture) leading to differing starting numbers of Fe(II)-oxidizing bacteria.

Optimum O_2 concentrations for the growth of microaerophilic Fe(II)-oxidizing bacteria are considered to be in the range of 5–20 μM, with relatively highest microbial contribution to overall Fe(II) oxidation at O_2 concentrations of 10 μM in the absence of initial Fe(III) minerals (Maisch et al., 2019). In liquid culture glass vials with a ferrihydrite-citrate mixture and incubation in UV light, Fe(II)-oxidizing bacteria contributed up to 40% of the overall Fe(II) oxidation after 24 h (Figure 4a inset). Their contribution decreased to 7% after 48 h incubation, probably due to increasing fast heterogeneous Fe(II) oxidation (Maisch et al., 2019; Park & Dempsey, 2005; Tamura et al., 1976), which increases the contribution of chemical Fe(II) oxidation to the overall Fe(II) oxidation. This indicates that, within the first 24 h, microaerophilic Fe(II)-oxidizing bacteria have the best growth conditions. However, the increase in 16S rRNA gene copy numbers provides a different measure of optimum growth conditions. After 48 h incubation of microaerophilic Fe(II)-oxidizers in liquid culture glass vials, a similar number of gene copies were quantified (approx. 7×10^7 ml^{-1}) during the incubation in UV as in blue light (Figure 4d). At that time, only 13% (UV light) or 5% (blue light) of the total Fe was still available as Fe(II) (Figure 4a), which corresponds to Fe(II) concentrations of approx. 90 or 40 μM, respectively. After 96 h incubation, this Fe(II) was completely removed (Figure 4a). Gene

copy numbers, however, strongly increased during the same time, reaching numbers of 2.3×10^8 ml^{-1} (UV light) and 1.6×10^8 ml^{-1} (blue light) (Figure 4d). There must therefore have been an ongoing Fe(III) reduction enabling that growth. As incubation in the dark did not reach these gene copy numbers (Figure 4d), light must have induced the Fe(II) formation and availability. Therefore, UV and blue light induced a cryptic iron cycle, at which no or only low net concentrations of Fe(II) could be quantified but cells grew. Cryptic cycling is characterized by rapid turnover of redox species (Hansel et al., 2015; Kappler & Bryce, 2017) making quantification of reduction and oxidation reactions difficult. The Fe(II) formed by Fe(III) photoreduction was immediately oxidized by O_2, either chemically or by microaerophilic Fe(II)-oxidizing bacteria. Hence, the quantifiable contribution of microaerophilic Fe(II)-oxidizers to the measurable overall net Fe(II) oxidation might not be a reliable measure for defining optimum growth conditions when Fe(II) production, for example, by Fe(III) photoreduction and abiotic and biotic Fe(II) oxidation run in parallel but increasing gene copy numbers must be taken into these considerations as well.

4.4 | Environmental implications

Microaerophilic Fe(II)-oxidizing bacteria are commonly found at anoxic–oxic interfaces in the environment, such as in stratified water columns (Field et al., 2016), in wetland rhizospheres (Weiss et al., 2003), or in freshwater and marine sediments (Laufer et al., 2016; Otte et al., 2018). Despite absorption of light, especially of UV light, by attenuating substances in water (Piazena et al., 2002), many of those environments are illuminated by sunlight, and Fe(III) photoreduction can be an important Fe(II) source if photoactive organic complexing agents are not limited (Lueder, Jørgensen, et al., 2020; Lueder, Maisch, et al., 2020). Fe(III)-complexing molecules such as low molecular weight organic acids (e.g., citrate) or humic substances are commonly found in natural environments (Jones, 1998; Mucha et al., 2005; Straub et al., 2005; Zhang & Yuan, 2017). Depending on their functional groups, formed Fe(III)-organic complexes can undergo Fe(III) photoreduction (Barbeau et al., 2003). The photoproduced Fe(II) is an electron donor for phototrophic Fe(II)-oxidizing bacteria (Peng et al., 2019) and, as shown here, for different microaerophilic Fe(II)-oxidizers. The microaerophilic Fe(II)-oxidizers are often more abundant than phototrophic Fe(II)-oxidizers in sediments (Laufer et al., 2016; Otte et al., 2018). Fe(III) photoreduction potentially expands the habitats of microaerophilic Fe(II)-oxidizing bacteria from the oxic–anoxic interfaces toward more oxic conditions, where Fe(II) is photoproduced. With Fe(III) photoreduction being an Fe(II) source in oxic, organic-rich, and light-influenced sediments on the one hand, and chemical and microaerophilic Fe(II) oxidation being an Fe(II) sink on the other hand, cryptic iron cycling expectedly takes place in many illuminated sediments. Fe(II) might not be measurable in the oxic zone because it undergoes rapid oxidation but we could show that microaerophilic Fe(II)-oxidizing bacteria are still able to grow using this Fe(II) as electron donor. Depending on prevalent conditions, microaerophilic Fe(II)-oxidizing bacteria can contribute up to 80% to overall Fe(II) oxidation (Chan et al., 2016). Considering that Fe(III) photoreduction may continuously deliver Fe(II), provided that sufficient photoactive organic complexing agents are present, the activity and relative contribution of microaerophilic Fe(II)-oxidizers to the overall Fe cycling may have been underestimated in illuminated environments so far.

5 | CONCLUSION

In illuminated, organic-rich sediments, Fe(II) is produced from abiotic Fe(III) photoreduction and provides optimum growth conditions for microaerophilic Fe(II)-oxidizing bacteria. This leads to rapid Fe redox turnover in the (micro)oxic surface zone (cryptic cycling) and impacts the biogeochemical Fe cycle. Microbial and abiotic Fe(III) reduction generally proceed in anoxic environments (Schmidt et al., 2010) and require electron donors such as sulfide, dihydrogen, or methane (Kappler et al., 2021). Fe(III) photoreduction, in contrast, takes place in the surface layer of organic-rich sediments. The process thereby expands the habitat of microaerophilic Fe(II)-oxidizing bacteria and enables Fe(III) reduction in the oxic zone. Thus, light not only influences the sedimentary Fe cycle but also directly impacts the carbon cycle by the oxidation of Fe(III)-complexing organic ligands during direct ligand-to-metal charge transfer reactions, eventually changing their bioavailability (Kaiser & Sulzberger, 2004; Pullin et al., 2004; Sulzberger & Durisch-Kaiser, 2009) or by forming reactive oxygen species (ROS) during light-induced reactions of photo-excited dissolved organic matter with O_2 (Cooper et al., 1988). Due to their high reactivity, ROS also couple other elemental cycles in the environment and thereby influence photosynthetic activity or microbial metabolism (Hansel et al., 2015).

More research is needed to determine the direct or indirect role of light and Fe(III) photoreduction for other Fe-metabolizing bacteria than phototrophic or microaerophilic Fe(II)-oxidizers. The impact of light in other environments than water columns or sediments, such as in soils, was not investigated so far and might have important consequences for various biogeochemical cycles as well.

ACKNOWLEDGEMENTS

The authors acknowledge infrastructural support by the Deutsche Forschungsgemeinschaft (DFG, German Research Foundation) under Germany's Excellence Strategy, cluster of Excellence EXC2124, project ID 390838134. This study was funded by the DFG to A.K. (grant KA 1736/57-1) and C.S. (grant SCHM2808/4-1). C.S. received additional funding from a Margarete von Wrangell fellowship (Ministry of Baden-Württemberg, Germany). We thank Franziska Schaedler for her support during molecular biology work and Natalia Jakus for scientific input concerning microaerophilic Fe(II)-oxidizing strains. The authors gratefully acknowledge the Tübingen Structural Microscopy Core Facility (Funded by the Federal Ministry of Education and Research (BMBF) and the Baden-Württemberg Ministry of Science

as part of the Excellence Strategy of the German Federal and State Governments) for their support & assistance in this work and thank the DFG (INST 37/1027-1 FUGG) for financial support provided for the acquisition of the cryogenic focused ion beam scanning electron microscope.

CONFLICT OF INTEREST

The authors declare no competing financial interest.

DATA AVAILABILITY STATEMENT

The data that support the findings of this study are available from the corresponding author upon reasonable request.

ORCID

Ulf Lueder https://orcid.org/0000-0003-0756-2447
Andreas Kappler https://orcid.org/0000-0002-3558-9500

REFERENCES

Abrahamson, H. B., Rezvani, A. B., & Brushmiller, J. G. (1994). Photochemical and spectroscopic studies of complexes, of iron(III) with citric acid and other carboxylic acids. *Inorganica Chimica Acta*, *226*, 117–127. https://doi.org/10.1016/0020-1693(94)04077-X

Barbeau, K. (2006). Photochemistry of organic iron(III) complexing ligands in oceanic systems. *Photochemistry and Photobiology*, *82*, 1505–1516. https://doi.org/10.1111/j.1751-1097.2006.tb09806.x

Barbeau, K., Rue, E. L., Trick, C. G., Bruland, K. W., & Butler, A. (2003). Photochemical reactivity of siderophores produced by marine heterotrophic bacteria and cyanobacteria based on characteristic Fe(III) binding groups. *Limnology and Oceanography*, *48*, 1069–1078. https://doi.org/10.4319/lo.2003.48.3.1069

Barnes, A., Sapsford, D. J., Dey, M., & Williams, K. P. (2009). Heterogeneous Fe(II) oxidation and zeta potential. *Journal of Geochemical Exploration*, *100*, 192–198. https://doi.org/10.1016/j.gexplo.2008.06.001

Bennett, J. H., Lee, E. H., Krizek, D. T., Olsen, R. A., & Brown, J. C. (1982). Photochemical reduction of iron. II. Plant related factors. *Journal of Plant Nutrition*, *5*, 335–344. https://doi.org/10.1080/01904168209362962

Brendel, P. J., & Luther, G. W. (1995). Development of a gold amalgam voltammetric microelectrode for the determination of dissolved Fe, Mn, O_2, and S(-II) in porewaters of marine and freshwater sediments. *Environmental Science and Technology*, *29*, 751–761. https://doi.org/10.1021/es00003a024

Bristow, G., & Taillefert, M. (2008). VOLTINT: A Matlab®-based program for semi-automated processing of geochemical data acquired by voltammetry. *Computers and Geosciences*, *34*, 153–162. https://doi.org/10.1016/j.cageo.2007.01.005

Bryce, C., Blackwell, N., Schmidt, C., Otte, J., Huang, Y. M., Kleindienst, S., Tomaszewski, E., Schad, M., Warter, V., Peng, C., Byrne, J. M., & Kappler, A. (2018). Microbial anaerobic Fe(II) oxidation – Ecology, mechanisms and environmental implications. *Environmental Microbiology*, *20*, 3462–3483. https://doi.org/10.1111/1462-2920.14328

Chan, C. S., Emerson, D., & Luther, G. W. (2016). The role of microaerophilic Fe-oxidizing micro-organisms in producing banded iron formations. *Geobiology*, *14*, 509–528. https://doi.org/10.1111/gbi.12192

Cohn, C. A., Pak, A., Strongin, D., & Schoonen, M. A. (2005). Quantifying hydrogen peroxide in iron-containing solutions using leuco crystal violet. *Geochemical Transactions*, *6*, 47. https://doi.org/10.1186/1467-4866-6-47

Cooper, W. J., Zika, R. G., Petasne, R. G., & Fischer, A. M. (1988). Sunlight-induced photochemistry of humic substances in natural waters: Major reactive species. In I. H. Suffet & Patrick MacCarthy (Eds.), *Aquatic humic substances, advances in chemistry* (pp. 333–362). American Chemical Society.

Davison, W., & Seed, G. (1983). The kinetics of the oxidation of ferrous iron in synthetic and natural waters. *Geochimica Et Cosmochimica Acta*, *47*, 67–79. https://doi.org/10.1016/0016-7037(83)90091-1

Dou, J., Alpert, P. A., Corral Arroyo, P., Luo, B., Schneider, F., Xto, J., Huthwelker, T., Borca, C. N., Henzler, K. D., Raabe, J., Watts, B., Herrmann, H., Peter, T., Ammann, M., & Krieger, U. K. (2021). Photochemical degradation of iron(III) citrate/citric acid aerosol quantified with the combination of three complementary experimental techniques and a kinetic process model. *Atmospheric Chemistry and Physics*, *21*, 315–338. https://doi.org/10.5194/acp-21-315-2021

Druschel, G. K., Emerson, D., Sutka, R., Suchecki, P., & Luther, G. W. (2008). Low-oxygen and chemical kinetic constraints on the geochemical niche of neutrophilic iron(II) oxidizing microorganisms. *Geochimica Et Cosmochimica Acta*, *72*, 3358–3370. https://doi.org/10.1016/j.gca.2008.04.035

Emerson, D., Fleming, E. J., & McBeth, J. M. (2010). Iron-oxidizing bacteria: An environmental and genomic perspective. *Annual Review of Microbiology*, *64*, 561–583. https://doi.org/10.1146/annurev.micro.112408.134208

Emerson, D., & Floyd, M. M. (2005). Enrichment and isolation of iron-oxidizing bacteria at neutral pH. In J. R. Leadbetter (Ed.), *Methods in enzymology* (pp. 112–123). Academic Press.

Emerson, D., & Moyer, C. (1997). Isolation and characterization of novel iron-oxidizing bacteria that grow at circumneutral pH. *Applied and Environmental Microbiology*, *63*, 4784–4792. https://doi.org/10.1128/aem.63.12.4784-4792.1997

Emerson, D., & Moyer, C. L. (2002). Neutrophilic Fe-oxidizing bacteria are abundant at the Loihi Seamount hydrothermal vents and play a major role in Fe oxide deposition. *Applied and Environmental Microbiology*, *68*, 3085–3093. https://doi.org/10.1128/AEM.68.6.3085-3093.2002

Emmenegger, L., Schönenberger, R., Sigg, L., & Sulzberger, B. (2001). Light-induced redox cycling of iron in circumneutral lakes. *Limnology and Oceanography*, *46*, 49–61. https://doi.org/10.4319/lo.2001.46.1.0049

Faust, B. C., & Zepp, R. G. (1993). Photochemistry of aqueous iron(III)-polycarboxylate complexes: Roles in the chemistry of atmospheric andsurface waters. *Environmental Science and Technology*, *27*, 2517–2522. https://doi.org/10.1021/es00048a032

Field, E. K., Kato, S., Findlay, A. J., MacDonald, D. J., Chiu, B. K., Luther, G. W., & Chan, C. S. (2016). Planktonic marine iron oxidizers drive iron mineralization under low-oxygen conditions. *Geobiology*, *14*, 499–508. https://doi.org/10.1111/gbi.12189

Gauger, T., Konhauser, K., & Kappler, A. (2015). Protection of phototrophic iron(II)-oxidizing bacteria from UV irradiation by biogenic iron(III) minerals: Implications for early Archean banded iron formation. *Geology*, *43*, 1067–1070. https://doi.org/10.1130/G37095.1

Gauger, T., Konhauser, K., & Kappler, A. (2016). Protection of nitrate-reducing Fe(II)-oxidizing bacteria from UV radiation by Biogenic Fe(III) minerals. *Astrobiology*, *16*, 301–310. https://doi.org/10.1089/ast.2015.1365

Gülay, A., Çekiç, Y., Musovic, S., Albrechtsen, H.-J., & Smets, B. F. (2018). Diversity of iron oxidizers in groundwater-fed rapid sand filters: Evidence of Fe(II)-dependent growth by *Curvibacter* and *Undibacterium* spp. *Frontiers in Microbiology*, *9*, 2808. https://doi.org/10.3389/fmicb.2018.02808

Hansel, C. M., Ferdelman, T. G., & Tebo, B. M. (2015). Cryptic cross-linkages among biogeochemical cycles: Novel insights from reactive intermediates. *Elements*, *11*, 409–414. https://doi.org/10.2113/gselements.11.6.409

Huang, J., Jones, A., Waite, T. D., Chen, Y., Huang, X., Rosso, K. M., Kappler, A., Mansor, M., Tratnyek, P. G., & Zhang, H. (2021). Fe(II) redox chemistry in the environment. *Chemical Reviews*, *121*, 8161–8233. https://doi.org/10.1021/acs.chemrev.0c01286

Jones, D. L. (1998). Organic acids in the rhizosphere - A critical review. *Plant and Soil*, *205*, 25–44.

Jørgensen, B. B., Cohen, Y., & Des, M. D. J. (1987). Photosynthetic action spectra and adaptation to spectral light distribution in a benthic cyanobacterial mat. *Applied and Environmental Microbiology*, *53*, 879–886. https://doi.org/10.1128/aem.53.4.879-886.1987

Kaiser, E., & Sulzberger, B. (2004). Phototransformation of riverine dissolved organic matter (DOM) in the presence of abundant iron: Effect on DOM bioavailability. *Limnology and Oceanography*, *49*, 540–554. https://doi.org/10.4319/lo.2004.49.2.0540

Kappler, A., & Bryce, C. (2017). Cryptic biogeochemical cycles: Unravelling hidden redox reactions. *Environmental Microbiology*, *19*, 842–846.

Kappler, A., Bryce, C., Mansor, M., Lueder, U., Byrne, J. M., & Swanner, E. D. (2021). An evolving view on biogeochemical cycling of iron. *Nature Reviews Microbiology*, *19*, 360–374. https://doi.org/10.1038/s41579-020-00502-7

Kato, S., Kikuchi, S., Kashiwabara, T., Takahashi, Y., Suzuki, K., Itoh, T., Ohkuma, M., & Yamagishi, A. (2012). Prokaryotic abundance and community composition in a freshwater iron-rich microbial mat at circumneutral pH. *Geomicrobiology Journal*, *29*, 896–905. https://doi.org/10.1080/01490451.2011.635763

King, D. W., Lounsbury, H. A., & Millero, F. J. (1995). Rates and mechanism of Fe(II) oxidation at nanomolar total iron concentrations. *Environmental Science and Technology*, *29*, 818–824. https://doi.org/10.1021/es00003a033

King, W. D., Aldrich, R. A., & Charnecki, S. E. (1993). Photochemical redox cycling of iron in NaCl solutions. *Marine Chemistry*, *44*, 105–120. https://doi.org/10.1016/0304-4203(93)90196-U

Kühl, M., Lassen, C., & Jørgensen, B. B. (1994). Light penetration and light intensity in sandy marine sediments measured with irradiance and scalar irradiance fiber-optic microprobes. *Marine Ecology Progress Series*, *105*, 139–148. https://doi.org/10.3354/meps105139

Kuma, K., Nakabayashi, S., & Matsunaga, K. (1995). Photoreduction of Fe(III) by hydroxycarboxylic acids in seawater. *Water Research*, *29*, 1559–1569. https://doi.org/10.1016/0043-1354(94)00289-J

Laufer, K., Nordhoff, M., Røy, H., Schmidt, C., Behrens, S., Jørgensen, B. B., & Kappler, A. (2016). Coexistence of microaerophilic, nitrate-reducing, and phototrophic Fe(II) oxidizers and Fe(III) reducers in coastal marine sediment. *Applied and Environmental Microbiology*, *82*, 1433–1447. https://doi.org/10.1128/AEM.03527-15

Lueder, U., Druschel, G., Emerson, D., Kappler, A., & Schmidt, C. (2018). Quantitative analysis of O_2 and Fe^{2+} profiles in gradient tubes for cultivation of microaerophilic Iron(II)-oxidizing bacteria. *FEMS Microbiology Ecology*, *94*(2). https://doi.org/10.1093/femsec/fix177

Lueder, U., Jørgensen, B. B., Kappler, A., & Schmidt, C. (2020). Fe(III) photoreduction producing Fe_{aq}^{2+} in oxic freshwater sediment. *Environmental Science and Technology*, *54*, 862–869.

Lueder, U., Jørgensen, B. B., Maisch, M., Schmidt, C., & Kappler, A. (2022). Influence of Fe(III) source, light quality, photon flux and presence of oxygen on photoreduction of Fe(III)-organic complexes – Implications for light-influenced coastal freshwater and marine sediments. *Science of the Total Environment*, *814*, 152767. https://doi.org/10.1016/j.scitotenv.2021.152767

Lueder, U., Maisch, M., Laufer, K., Jørgensen, B. B., Kappler, A., & Schmidt, C. (2020). Influence of physical perturbation on Fe(II) supply in coastal marine sediments. *Environmental Science and Technology*, *54*, 3209–3218. https://doi.org/10.1021/acs.est.9b06278

Macdonald, D. J., Findlay, A. J., McAllister, S. M., Barnett, J. M., Hredzak-Showalter, P., Krepski, S. T., Cone, S. G., Scott, J., Bennett, S. K., Chan, C. S., Emerson, D., & Luther, G. W. (2014). Using in situ voltammetry as a tool to identify and characterize habitats of iron-oxidizing bacteria: From fresh water wetlands to hydrothermal vent sites. *Environmental Sciences: Processes and Impacts*, *16*, 2117–2126.

Maisch, M., Lueder, U., Laufer, K., Scholze, C., Kappler, A., & Schmidt, C. (2019). Contribution of microaerophilic iron(II)-oxidizers to iron(III) mineral formation. *Environmental Science and Technology*, *53*, 8197–8204. https://doi.org/10.1021/acs.est.9b01531

McBeth, J. M., Little, B. J., Ray, R. I., Farrar, K. M., & Emerson, D. (2011). Neutrophilic iron-oxidizing "Zetaproteobacteria" and mild steel corrosion in nearshore marine environments. *Applied and Environmental Microbiology*, *77*, 1405–1412.

Miller, W. L., & Kester, D. (1994). Photochemical iron reduction and iron bioavailability in seawater. *Journal of Marine Research*, *52*(2), 325–343. https://doi.org/10.1357/0022240943077136

Millero, F. J., Sotolongo, S., & Izaguirre, M. (1987). The oxidation kinetics of Fe(II) in seawater. *Geochimica Et Cosmochimica Acta*, *51*, 793–801. https://doi.org/10.1016/0016-7037(87)90093-7

Mottola, H. A., Simpson, B. E., & Gorin, G. (1970). Absorptiometric determination of hydrogen peroxide in submicrogram amounts with leuco crystal violet and peroxidase as catalyst. *Analytical Chemistry*, *42*, 410–411. https://doi.org/10.1021/ac60285a017

Mucha, A. P., Almeida, C. M. R., Bordalo, A. A., & Vasconcelos, M. T. S. D. (2005). Exudation of organic acids by a marsh plant and implications on trace metal availability in the rhizosphere of estuarine sediments. *Estuarine, Coastal and Shelf Science*, *65*, 191–198. https://doi.org/10.1016/j.ecss.2005.06.007

Nadkarni, M. A., Martin, F. E., Jacques, N. A., & Hunter, N. (2002). Determination of bacterial load by real-time PCR using a broad-range (universal) probe and primers set. *Microbiology*, *148*, 257–266. https://doi.org/10.1099/00221287-148-1-257

Neubauer, S. C., Emerson, D., & Megonigal, J. P. (2002). Life at the energetic edge: Kinetics of circumneutral iron oxidation by lithotrophic iron-oxidizing bacteria isolated from the wetland-plant rhizosphere. *Applied and Environmental Microbiology*, *68*, 3988–3995. https://doi.org/10.1128/AEM.68.8.3988-3995.2002

Otte, J. M., Harter, J., Laufer, K., Blackwell, N., Straub, D., Kappler, A., & Kleindienst, S. (2018). The distribution of active iron-cycling bacteria in marine and freshwater sediments is decoupled from geochemical gradients. *Environmental Microbiology*, *20*, 2483–2499. https://doi.org/10.1111/1462-2920.14260

Park, B., & Dempsey, B. A. (2005). Heterogeneous oxidation of Fe(II) on ferric oxide at neutral pH and a low partial pressure of O_2. *Environmental Science and Technology*, *39*, 6494–6500.

Pehkonen, S. O., Siefert, R., Erel, Y., Webb, S., & Hoffmann, M. R. (1993). Photoreduction of iron oxyhydroxides in the presence of important atmospheric organic compounds. *Environmental Science and Technology*, *27*, 2056–2062. https://doi.org/10.1021/es00047a010

Peng, C., Bryce, C., Sundman, A., & Kappler, A. (2019). Cryptic cycling of complexes containing Fe(III) and organic matter by phototrophic Fe(II)-oxidizing bacteria. *Applied and Environmental Microbiology*, *85*, e02826–e2918. https://doi.org/10.1128/AEM.02826-18

Pfennig, N. (1978). *Rhodocyclus purpureus* gen. nov. and sp. nov., a ring shaped, vitamin B12 requiring member of the family *Rhodospirillaceae*. *International Journal of Systematic Bacteriology*, *28*, 283–288. https://doi.org/10.1099/00207713-28-2-283

Piazena, H., Perez-Rodrigues, E., Häder, D. P., & Lopez-Figueroa, F. (2002). Penetration of solar radiation into the water column of the central subtropical Atlantic Ocean - Optical properties and possible biological consequences. *Deep-Sea Research Part II: Topical Studies in Oceanography*, *49*, 3513–3528. https://doi.org/10.1016/S0967-0645(02)00093-0

Pullin, M. J., Bertilsson, S., Goldstone, J. V., & Voelker, B. M. (2004). Effects of sunlight and hydroxyl radical on dissolved organic matter: Bacterial growth efficiency and production of carboxylic acids and other substrates. *Limnology and Oceanography*, *49*, 2011–2022.

Rijkenberg, M. J. A., Fischer, A. C., Kroon, J. J., Gerringa, L. J. A., Timmermans, K. R., Wolterbeek, H. T., & De, B. H. J. W. (2005). The influence of UV irradiation on the photoreduction of iron in the Southern Ocean. *Marine Chemistry*, *93*, 119–129. https://doi.org/10.1016/j.marchem.2004.03.021

Rose, A. L., & Waite, T. D. (2005). Reduction of organically complexed ferric iron by superoxide in a simulated natural water. *Environmental Science and Technology*, *39*, 2645–2650. https://doi.org/10.1021/es048765k

Schmidt, C., Behrens, S., & Kappler, A. (2010). Ecosystem functioning from a geomicrobiological perspective a conceptual framework for biogeochemical iron cycling. *Environmental Chemistry*, *7*, 399–405. https://doi.org/10.1071/EN10040

Slowey, A. J., & Marvin-DiPasquale, M. (2012). How to overcome inter-electrode variability and instability to quantify dissolved oxygen, Fe(II), mn(II), and S(−II) in undisturbed soils and sediments using voltammetry. *Geochemical Transactions*, *13*, 6. https://doi.org/10.1186/1467-4866-13-6

St Clair, B., Pottenger, J., Debes, R., Hanselmann, K., & Shock, E. (2019). Distinguishing biotic and abiotic iron oxidation at low temperatures. *ACS Earth and Space Chemistry*, *3*, 905–921. https://doi.org/10.1021/acsearthspacechem.9b00016

Stookey, L. L. (1970). Ferrozine - A new spectrophotometric reagent for iron. *Analytical Chemistry*, *42*, 779–781. https://doi.org/10.1021/ac60289a016

Straub, K. L., Kappler, A., & Schink, B. (2005). Enrichment and isolation of ferric-iron- and humic-acid-reducing bacteria. In J. R. Leadbetter (Ed.), *Methods in enzymology* (pp. 58–77). Academic Press.

Sulzberger, B., & Durisch-Kaiser, E. (2009). Chemical characterization of dissolved organic matter (DOM): A prerequisite for understanding UV-induced changes of DOM absorption properties and bioavailability. *Aquatic Sciences*, *71*, 104–126. https://doi.org/10.1007/s00027-008-8082-5

Sulzberger, B., Suter, D., Siffert, C., Banwart, S., & Stumm, W. (1989). Dissolution of Fe(III)(hydr)oxides in natural waters; laboratory assessment on the kinetics controlled by surface coordination. *Marine Chemistry*, *28*, 127–144. https://doi.org/10.1016/0304-4203(89)90191-6

Swanner, E. D., Nell, R. M., & Templeton, A. S. (2011). *Ralstonia* species mediate Fe-oxidation in circumneutral, metal-rich subsurface fluids of Henderson mine, CO. *Chemical Geology*, *284*, 339–350. https://doi.org/10.1016/j.chemgeo.2011.03.015

Tamura, H., Goto, K., & Nagayama, M. (1976). The effect of ferric hydroxide on the oxygenation of ferrous ions in neutral solutions. *Corrosion Science*, *16*, 197–207. https://doi.org/10.1016/0010-938X(76)90046-9

Tschech, A., & Pfennig, N. (1984). Growth yield increase linked to caffeate reduction in *Acetobacterium woodii*. *Archives of Microbiology*, *137*, 163–167. https://doi.org/10.1007/BF00414460

Waite, T. D., Szymczak, R., Espey, Q. I., & Furnas, M. J. (1995). Diel variations in iron speciation in northern Australian shelf waters. *Marine Chemistry*, *50*, 79–91. https://doi.org/10.1016/0304-4203(95)00028-P

Weiss, J. V., Emerson, D., Backer, S. M., & Megonigal, J. P. (2003). Enumeration of Fe(II)-oxidizing and Fe(III)-reducing bacteria in the root zone of wetland plants: Implications for a rhizosphere iron cycle. *Biogeochemistry*, *64*, 77–96.

Widdel, F., Schnell, S., Heising, S., Ehrenreich, A., Assmus, B., & Schink, B. (1993). Ferrous iron oxidation by anoxygenic phototrophic bacteria. *Nature*, *362*, 834–836. https://doi.org/10.1038/362834a0

Zhang, P., & Yuan, S. (2017). Production of hydroxyl radicals from abiotic oxidation of pyrite by oxygen under circumneutral conditions in the presence of low-molecular-weight organic acids. *Geochimica Et Cosmochimica Acta*, *218*, 153–166. https://doi.org/10.1016/j.gca.2017.08.032

How to cite this article: Lueder, U., Maisch, M., Jørgensen, B. B., Druschel, G., Schmidt, C., & Kappler, A. (2022). Growth of microaerophilic Fe(II)-oxidizing bacteria using Fe(II) produced by Fe(III) photoreduction. *Geobiology*, 20, 421–434. https://doi.org/10.1111/gbi.12485